catalysts

MDPI

Article

Effect of Surface Composition and Structure of the Mesoporous Ni/KIT-6 Catalyst on Catalytic Hydrodeoxygenation Performance

Xianming Zhang [1,*,†], Shuang Chen [1,†], Fengjiao Wang [2], Lidan Deng [2], Jianmin Ren [2], Zhaojie Jiao [1] and Guilin Zhou [1,2,*]

1 Engineering Research Center for Waste Oil Recovery Technology and Equipment, Ministry of Education, Chongqing Technology and Business University, Chongqing 400067, China; chenshuang023@gmail.com (S.C.); jiaozhaojie2001@ctbu.edu.cn (Z.J.)

2 Department of Materials Science and Engineering, Chongqing Technology and Business University, Chongqing 400067, China; wfj1122345@163.com (F.W.); dld2006lidan@163.com (L.D.); renjianmin123@sohu.com (J.R.)

* Correspondence: zxm215@126.com (X.Z.); dicpglzhou@ctbu.edu.cn (G.Z.); Tel.: +86-23-62769-785

† These authors contributed equally to this work and should be considered co-first authors.

Received: 13 October 2019; Accepted: 22 October 2019; Published: 25 October 2019

Abstract: A series of Ni/KIT6 catalyst precursors with 25 wt.% Ni loading amount were reduced in H_2 at 400, 450, 500, and 550 °C, respectively. The studied catalysts were investigated by XRD, Quasi in-situ XPS, BET, TEM, and H_2-TPD/Ranalysis methods. It was found that reduction temperature is an important factor affecting the hydrodeoxygenation (HDO) performance of the studied catalysts because of the Strong Metal Support Interaction Effect (SMSI). The reduction temperature influences mainly the content of active components, crystal size, and the abilityfor adsorbing and activating H_2. The developed pore structure and large specific surface area of the KIT-6 support favored the Ni dispersion. The RT450 catalyst, which was prepared in H_2 atmosphere at 450 °C, has the best HDO performance. Ethyl acetate can be completely transformed and maintain 96.8% ethane selectivity and 3.2% methane selectivity at 300 °C. The calculated apparent activation energies of the prepared catalysts increased in the following order: RT550 > RT400 > RT500 > RT450.

Keywords: hydrodeoxygenation; Ni/KIT-6; ethyl acetate

1. Introduction

With the process of economic globalization, the energy demand is increasing in human society [1]. The development of non-renewable energyhasnot fully met the developmentneeds of industry and society [2,3]. Therefore, finding a reliable alternative energy product is imminent. In order to cope with the above energy crisis, the new green energy concept and energy conversion technology have been put forward. The use of fed oil to prepare biodiesel is one of the most effective ways to reduce the supply pressure of petrochemical diesel [4]. The edible oil mainly includes vegetable oil and animal oil, which are mainly composed of fatty acid or ester with long chain. Fatty acid or ester usually contains rich carbon resources with C_{12}–C_{24} bonds [5,6]. Therefore, the successful transformation of fed oil to biodiesel may effectively mitigate the current tense energy situation. At present, the first-generation biodiesel cannot completely be deoxygenated due to technical limitations. The products contain high oxygen content, resulting in low calorific value and poor adaptability [7–9]. In contrast, the second-generation biodiesel can be completely deoxygenated because of technical advantages, and the prepared product has excellent performance. The second-generation biodiesel produced by HDO technology is closer to the petrochemical diesel in physical and chemical properties than the first-generation biodiesel.

Therefore, HDO technology has attracted wide attention because of the important applicable value. Of course, it also will play adominant role in promoting the chemical industry in the future.

The research and development of high performance catalytic materials is the core of the HDO technology. At present, the most widely used catalytic materials are the supported noble metal catalysts, such as Pt [10], Pd [11], Ru [12], and so on. Pd/C catalyst has high yield of alkane products, which are used in the stearic acid HDO reaction. The yield of *n*-C_{17} alkane is over 60%, olefins and polymers are also produced with these products [13]. Yang et al. [14] prepared Pt/ZIF-67/zeolite 5A catalyst for oleic acid HDO and found that the oleic acid is completely transformed at 320 °C/2.0 MPa when Pt loading is only 0.5% due to the special structure of the studied catalyst. Good at stearic acid HDO reaction is 2% Ru/TiO_2. The results show that the product is composed of C_{17} and octadecanol whose selectivities are 18.1% and 78.2%, respectively, which indicates the product is the hydrolyzate product, and the hydrolysis rate is greater than the HDO rate [15]. Chen et al. [16] reports that the Ru/zeolite catalyst is used in the HDO study of fatty acid methyl ester. It is found that the fed oil mainly goes through decarbonylation pathway. At 300 °C/3.0 MPa, the fed oil conversion reaches 90.8%, and the selectivity of C_{17} reaches 64.3%. As is well known, the main advantage of the noble metal catalyst is the high catalytic activity, that is, the HDO reaction can be achieved at a relatively low reaction temperature. Nevertheless, noble metal catalysts are expensive. Therefore, transition metal catalyst has attracted much attention in the research and application in the HDO field. HDO and hydrodesulfurization have many similar characteristics; therefore, HDO catalysts are originally developed primarily as hydrodesulfurization catalysts. Kubicka et al. [17] use the CoMoS/MCM-41 to catalyze the HDO reaction of rapeseed oil in a fluidized bed, mainly obtaining the diesel components such as C_{17} and C_{18}, under the condition of 300~320 °C, 2.0–11.0 MPa, and 1.0–4.0 h^{-1}. The introduction of S element is conducive to preventing catalyst from being poisoned and even reducing some negative factors such as carbon deposition [18]. However, the S element may also be introduced into the product to reduce the environmental protection of the corresponding product [19]. Therefore, sulfur-free catalysts are getting more and more attention. Imane Hachemi et al. [20] use the sulfur-free Ni/γ-Al_2O_3 catalyst for the fatty acids HDO. Under 300 °C/3.0 MPa, 6.0 h is running stably. The selectivity of C_{17} reaches 96.2%, while the conversion of fatty acid reaches 100%. Mesoporous silicon-based materials have developed mesoporous structure and large specific surface area, which facilitates the active component in high dispersion on the support surface [21–23]. Therefore, replacing traditional support with mesoporous silicon-based material is a good method to solve the above problems we have met at the moment. At the same time, the use of ethyl acetate as a model compound can even effectively eliminate the influence of long chain alkyl structures over the studied catalytic HDO performance, thus obtaining more accurate information on HDO of oxygen containing functional groups [24,25]. As we all know, the reduction temperature can affect the valence state of the variable valence transition metal species, then influence the activation ability of the corresponding catalysts for oxygen containing functional groups in the ester molecules and H_2 molecules in the reaction system. Zs. Ferencz et al. [26] studied the reduction of Co/Al_2O_3 catalyst at different reduction temperatures. It was found that the composition of the corresponding catalyst is obviously affected by the reduction temperature. The higher the reduction temperature is, the more the Co content is. Furthermore, the higher the temperature is, the narrower the particle size distribution is. Therefore, the reduction temperature of the studied catalyst is a very important factor in the hydrogen reaction. However, the impact of the reduction temperature of Ni/KIT-6 catalyst on its HDO properties has rarely been reported.

In this paper, a series of 25 wt.% Ni/KIT-6 catalysts at different reduction temperatures. Ethyl acetate was used as model compound to investigate the catalytic HDO performance of the studied catalysts. The morphology structure, chemical composition, and physicochemical properties of the prepared catalysts were studied by means of XRD, Quasi in situ XPS, BET, TEM, and H_2-TPD.

2. Results and Discussion

2.1. H_2-TPR Studies

Figure 1 is the H_2-TPR spectrum of calcined precursor and pure NiO. It is known from Figure 1 that there is an obvious hydrogen consumption phenomenon when the reduction temperature reaches 100 °C. With the increase of the temperature, the catalyst precursor, at 185, 345, 390, and 530 °C, forms distinct hydrogen consumption peaks which are labeled as α, β, γ, and δ. Interestingly, the hydrogen consumption peak of the pure phase NiO sample appears at 410 °C, and the pure phase NiO sample has only one peak.

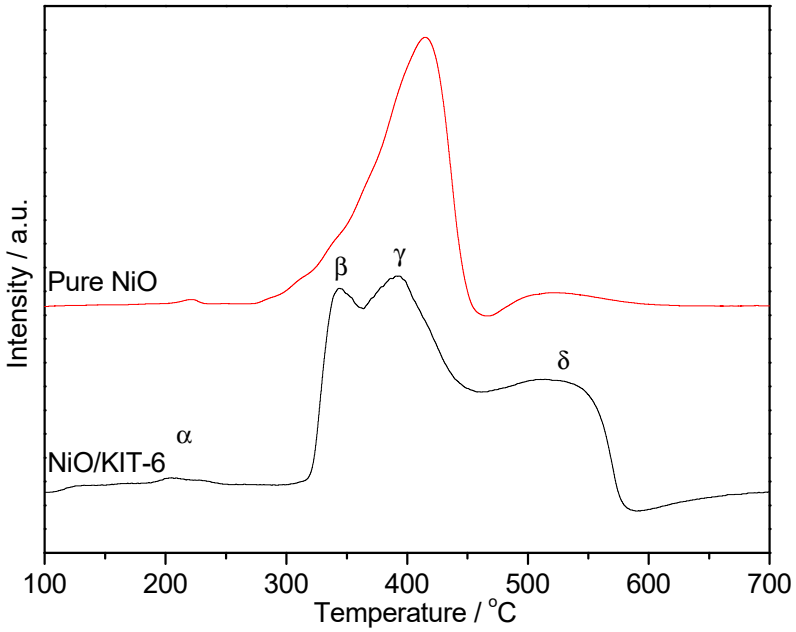

Figure 1. H_2-TPR patterns of catalyst precursor and pure NiO.

KIT-6 support has large specific surface area and developed pore structure, which can effectively promote the dispersion of NiO species. The H_2 reduction of highly dispersed NiO species forms α hydrogen consumption peak because of the preferred reducibility. The β hydrogen consumption peak is mainly attributed to the reduction of the dispersed NiO species on the surface. The interaction between this partial NiO and support SiO_2 is weak, thus showing good low temperature reducibility. The subsurface NiO species in the precursor is covered by the surface NiO species and has a certain interaction with the surface SiO_2. Therefore, the subsurface NiO species show a poor reducibility, and the reduction hydrogen consumption peak γ is formed in a higher temperature region than that of the surface NiO species. At the same time, the reduction peak at 530 °C may be attributed to the reduction of the NiO species in the support pore structure or the $NiSiO_3$ species formed at high temperature. The confinement and attachment effects of the nanopore structure hinder the reduction of partial NiO species in the channel. Moreover, this partial NiO species even may block the pore structure to restrict the diffusion and migration of H_2 flow in the pore structure, resulting in the reduction of NiO species in the higher temperature region. The confinement effect of KIT-6 pore structure enhances the interaction between NiO species and SiO_2 in the channel, leading to forming more stable NiO or $NiSiO_3$ species, which increase the difficulty of reduction. As a result, the large specific surface area and developed pore structure of the KIT-6 support can promote the NiO species to be highly dispersed, thus promoting the reduction of NiO species in the NiO/KIT-6 precursor. In addition, the results indicate that the NiO/KIT-6 precursor can be effectively reduced to prepare Ni/KIT-6 catalyst when the reduction temperature is 450 °C. However, there may still be some Ni^{2+} species (such as, NiO and $NiSiO_3$) that cannot be reduced by hydrogen at 450 °C.

2.2. XRD Characterization

The XRD spectra of the catalysts, which were produced by H_2 reduction at different temperatures, are shown in Figure 2. RT400, RT450, RT500, and RT550 catalysts form a series of XRD diffraction peaks at 2θ = 44.51, 51.81, and 76.41°, which corresponds to the face-centered cubic phase of metallic Ni (JCPDS NO. 04-0850) with {111}, {200}, and {220} planes, respectively [27]. In addition, the intensity of the metallic Ni diffraction peak is related to the reduction temperature. There is no other characteristic diffraction peak in the prepared catalysts expect for RT400 obtained by H_2 reduction at 400 °C for 2.0 h. In addition to the diffraction peak of the metallic Ni, the RT400 catalyst forms NiO peaks corresponding to the {111} and {220} planes at 2θ = 37.28 and 62.62°, using standard data (JCPDS No. 44-1159) [28]. The diffraction peaks of NiO phase have not been observed in RT450, RT500, and RT550 catalysts.

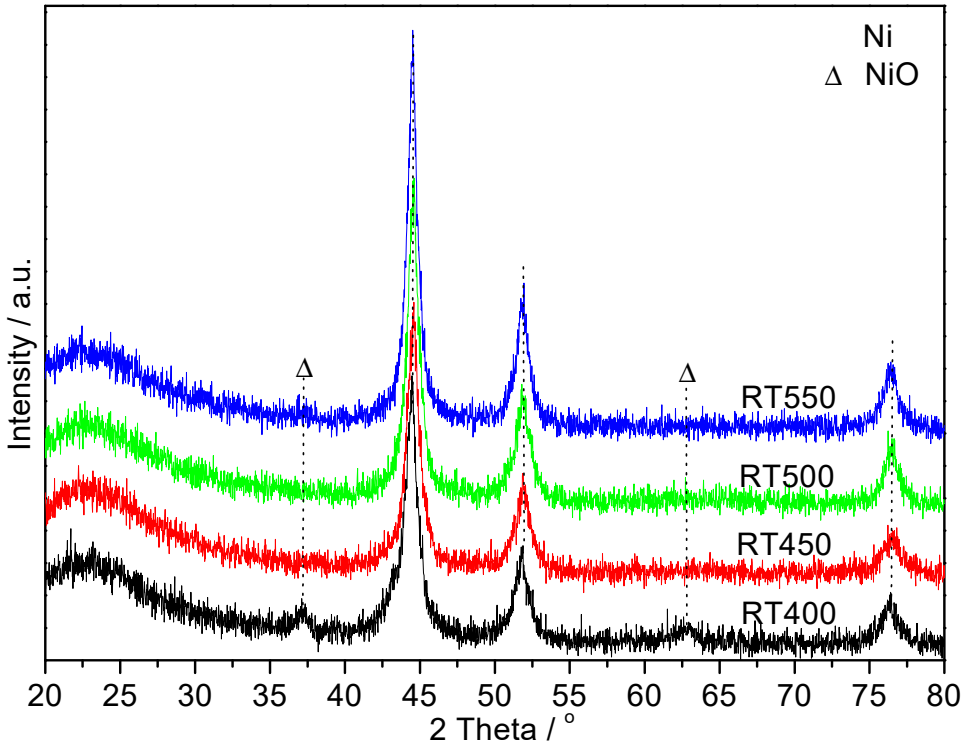

Figure 2. XRD patterns of RTx catalysts. (x = 400, 450, 500, and 550).

After reducing precursors at different temperatures, NiO species in precursors can be effectively reduced by H_2 to form metallic Ni species. The reduction temperature directly affects the reduction degree of NiO species, crystallinity, and dispersion of the metallic Ni species. Non reductive NiO species in the RT400 catalyst may belong to the NiO species that exist in the KIT-6 support pore structure. Meanwhile, the intensity of XRD diffraction peak of metallic Ni increases with increasing reduction temperature. The high reduction temperature can promote the migration and aggregation of metallic Ni to form stable Ni particles with large crystal size. Calculated by the Scherrer equation, the metallic Ni crystal sizes of the RT400, RT450, RT500, and RT550 catalysts are 5.9, 7.4, 9.1, and 10.0 nm, respectively (see Table 1). Under the heat dissipation action of H_2 flow, the migration and accumulation rate of metallic Ni during the reduction process of NiO/KIT-6 precursor can be decreased, thus, the high dispersion of metallic Ni crystal is maintained when the complete reduction is achieved. The lower reduction temperature is, the slower reduction rate of NiO species is. This can also be beneficial to the refinement of the metallic Ni crystal size. By contrary, at high reduction temperature, the effect of H_2 flow is not enough to prevent the high temperature sintering of metallic Ni, which reduces the dispersion and increases the crystal size. The reduction rate of NiO species is accelerated when the reduction temperature is too high, so that the formed metallic Ni particles with high surface energy can

overcome the limitation of the support structure and migrate to the surface of the support [24]. At this time, the metallic Ni exists on the support surface with supersaturated state; unfortunately, the crystal size increases gradually [29]. Therefore, too high reduction temperature will lead to the aggregation of metallic Ni, which may cause excessive crystallization of metallic Ni active components and even decrease the number of exposed active sites to affect the catalytic performance. At the high reduction temperature, the metallic Ni component may even produce a crystal surface that is not conducive to the HDO reaction. The XRD results are also confirmed that the NiO species can be effectively reduced by H_2 at 450 °C for 2.0 h to form metallic Ni. This result is consistent with the previous H_2-TPR results and previous reports [24,30]. However, there may still be some amorphous NiO or/and $NiSiO_3$ species, which formed at high-temperature calcination. What is more, it is also possible that the amount of NiO or/and $NiSiO_3$ is lower than the detection limit of XRD. This is probably the reason why NiO or/and $NiSiO_3$ has not been observed in RT450, RT500, and RT550 catalysts in XRD spectra.

Table 1. Physicochemical properties of RTx catalysts.

Catalyst	Crystal Size from XRD (nm) [a]	H_2-TPD (α Region) Quantity (μmol/g)	Surface Area (m^2/g) [b]	Average Pore Diameter (nm) [c]	Total Pore Volume (cm^3/g) [d]	Particle Size from TEM (nm) [e]
RT400	5.9	27.6	349.2	6.08	0.55	6.3
RT450	7.4	65.8	348.9	6.35	0.56	7.7
RT500	9.1	52.4	347.7	6.17	0.54	9.7
RT550	10	49.9	343.4	6.03	0.56	10.3
KIT-6	—	—	562.5	6.56	1.22	—

[a] Average Ni crystal diameter calculated from Ni(111) plane using Scherrer equation from XRD. [b] Calculated by the BET equation. [c] BJH adsorption average pore diameter. [d] BJH adsorption pore volume. [e] Average Ni particle size observed from TEM images.

2.3. Quasi In-Situ XPS Studies

Quasi in-situ XPS technology is mainly used to analyze surface elements and the state of the surface elements of the studied RTx catalysts. The XPS spectra of Ni 2p for RTx catalysts are shown in Figure 3. The peaks of Ni 2p at 856.5 and 852.7 eV are attributed to Ni^{2+} and Ni^0 species, respectively [29,31]. From the results of in situ XPS, it is found that the RTx catalysts have rich metallic Ni species, which indicates that Ni^{2+} in the catalyst precursors can be effectively reduced to metallic Ni active species. The results are similar to that of the XRD studies. Ni^{2+} species may originate from the amorphous NiO species in the pore structure or the $NiSiO_3$ species formed at high-temperature calcination or/and reduction. However, the peak area and intensity corresponding to Ni^0 are different in the RTx catalysts, which can be attributed to the interactions between the active component and the KIT-6 support having significant difference in the function of the different reduction temperatures.

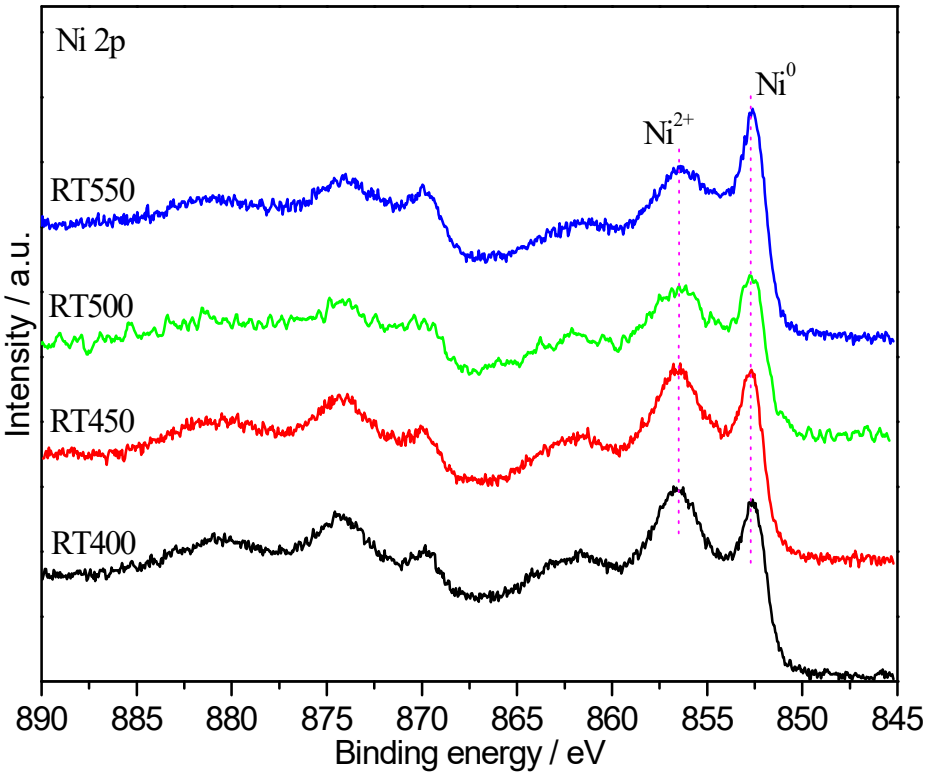

Figure 3. Spectra of the RTx catalysts. (x = 400, 450, 500, and 550).

2.4. H_2-TPD Studies

The H_2-TPD spectra of the studied RT400, RT450, RT500, and RT550 catalysts, which were reduced at different temperatures, are shown in Figure 4. It is known from Figure 4 that the prepared Ni based catalysts have good hydrogen desorption capacities and mainly form two hydrogen desorption regions, which are recorded as α and β, respectively. There are significant differences in the peak area and strength on the H_2-TPD patterns of the studied Ni/KIT-6 catalysts prepared at different reduction temperatures. The area of α peak increases with the increase of the reduction temperature and then decreases, and RT450 catalyst has the largest area of α peak among that of RTx catalysts. Conversely, the area and desorption temperature of β peak increase with the increase of the reduction temperature. The RT400 catalyst has a significant γ peak, mainly for the desorption of the bulk hydrogen species, which can store and supply the reactive hydrogen species for the reaction.

H_2-TPD can be used to effectively study the adsorption of H_2 molecules by corresponding catalyst and the ability to provide reactive hydrogen species for the HDO reaction [32]. Hydrogen species exist on the surface and in the bulk of the prepared Ni-based catalyst after reduction, and the physically adsorbed hydrogen species on the catalyst surface have been removed by Ar purge. In contrast, the chemisorbed hydrogen species are difficult to remove at room temperature by Ar purge because of the formation of a chemical bond between chemisorbed hydrogen species and metallic Ni active center. Therefore, the α and β hydrogen desorption regions formed by the catalysts can be attributed to the desorption of surface chemisorbed hydrogen species and metal hydride [24,32]. As is well known, the chemisorbed hydrogen species can also be effectively desorbed to form the reactive hydrogen species, which is required for the reaction by increasing the system temperature. Moreover, the bond energy of the chemisorbed hydrogen species is relatively weak, so it can be desorbed at low temperature (<400 °C). Unfortunately, compared with the chemisorbed hydrogen species, metal hydrides need to be decomposed at a higher temperature to release the hydrogen species. KIT-6 support has developed mesoporous structure, so Ni active components can penetrate into the inner surface, which helps to form active centers with different strength. H_2 molecules can also be adsorbed on the inner surface

of the studied Ni/KIT-6 catalyst, which is concluded as weakly and strongly adsorbed hydrogen. According to the XRD and quasi in situ XPS results, a small amount of non-reductive NiO species exist in the RT400 catalyst, which is not conducive to the formation of the active center in the catalyst. As a result, the adsorption capacity of H_2 decreases on the RT400 catalyst, resulting in a poor low temperature desorption ability of H_2. After elevating the reduction temperature, α region of the RT450 catalyst has the maximum peak area among the studied RTx catalysts. These findings suggest that the RT450 catalyst has the best hydrogen adsorption storage capacity, which can provide more reactive hydrogen species for the HDO reaction. By continuing to increase the reduction temperature of the prepared catalyst, the area of the α hydrogen desorption region gradually decreases, which is attributed to the gradual weakening of the hydrogen adsorption and storage capacity of the corresponding catalysts. The XRD results also confirm that the crystal size of Ni increases with the increase of the reduction temperature. However, the large crystal size leads to reducing the exposed active crystal surface. Moreover, the large crystal size is not conducive to the formation or fracture of the "Ni-H" species, thus weakening the adsorption and activation ability of the catalyst for the H_2 molecules. The area of the β region increases with the increase of the reduction temperature; the desorption peak temperature increases gradually. This find may suggest that the formed hydrogen species in the high temperature region are mainly due to the decomposition of the metal hydride; the stable metal hydride is more easily formed at higher reduction temperature.

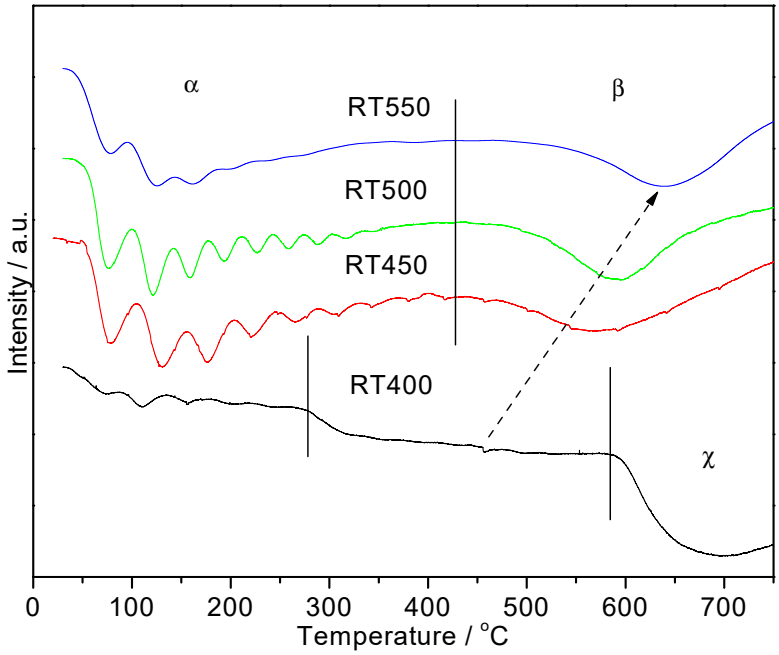

Figure 4. H_2-TPD patterns of RTx catalysts. (x = 400, 450, 500, and 550).

2.5. BET Characteristics

The porosities of the prepared RT400, RT450, RT500, and RT550 catalysts and KIT-6 support were studied by BET, as shown in Figure 5. The pore size distributions of the corresponding catalysts and KIT-6 support, calculated from the adsorption isotherm, were shown in the inset in Figure 5. All prepared RTx catalysts have a type IV isotherms with clear H1-type hysteresis loop, which indicates the corresponding catalysts have mesoporous structure. The specific surface area, pore volume, and pore diameter of the prepared catalysts are showed in Table 1. The prepared catalysts have inherited the developed pore structure of the KIT-6 support. Unfortunately, compared with the KIT-6 support, the specific surface area, pore volume, and pore diameter of the corresponding catalysts obviously decrease. These findings can be attributed to the loading of metallic Ni species entering the pore structure of KIT-6, resulting in the blockage of the pore structure. At the same time, the loading of

Ni species also reduces the support content in the unit volume or unit mass catalyst, which leads to decreasing the specific surface area of the corresponding catalyst. The results of Table 1 show that the RTx catalysts obtained at different reduction temperatures have maintained a specific surface area of about 340 m^2/g, the pore size also around 6 nm. It can be known that the change of the reduction temperature does not have a significant effect on the structure of the prepared catalysts. Because the high temperature accelerates the agglomeration of crystal and the increase of crystal size, the specific surface area has a slightly decrease by elevating the reduction temperature. However, the average pore diameter and total pore volume have not been affected by elevating the reduction temperature; that is to say, in the studied temperature region, the average pore diameter and total pore volume have no obvious rule to be observed by increasing reduction temperature. The pore diameter range is 6.03–6.35 nm, which is close to the pore diameter of KIT-6 support as showing in the Table 1. Based on the BET results, the developed pore structure and large specific surface area of KIT-6 contribute to support metallic Ni on its inner and outer surface, which leads to the metallic Ni in a high dispersion state and may even reach monolayer dispersion. With the filling and attachment of the metallic Ni on the KIT-6 inner surface, the micropore may be blocked, while the macropore structure can be filled to form mesopore structure. The reduction temperature can only change the chemical state and crystal size of Ni species; fortunately, it cannot change the structure of KIT-6 support. Therefore, the pore structure can maintain the pore size distribution and pore volume because of its confinement and attachment effects [24]. The slight changes of average pore diameter and total pore volume are mainly due to the growth of metal Ni crystal in the pore structure.

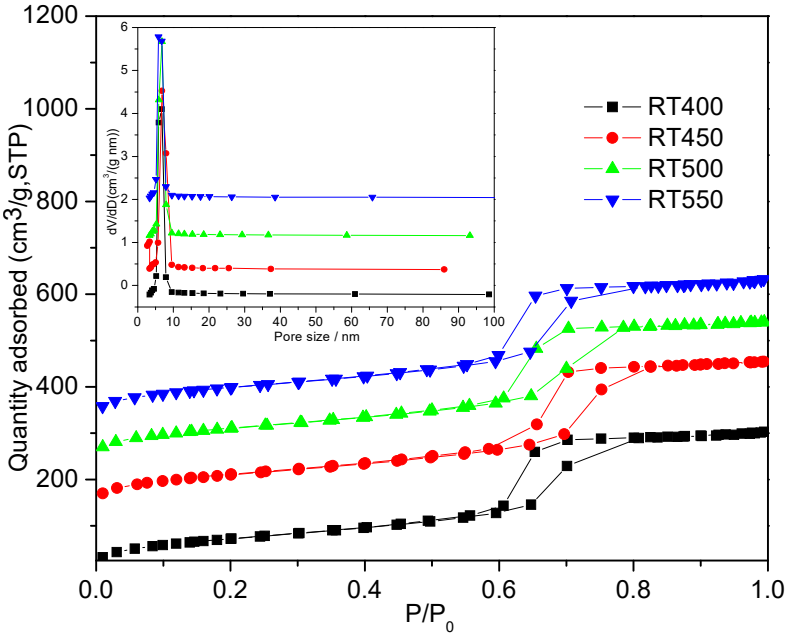

Figure 5. N_2 adsorption-desorption isotherms and pore diameter distributions of the prepared RTx catalysts. (x = 400, 450, 500, and 550).

2.6. TEM Characteristics

The prepared Ni/KIT-6 catalysts were studied by TEM, as shown in Figure 6. The prepared catalysts have obvious mesoporous structure, which is similar to that of the BET results. The metal Ni mainly presents two states. Some of the metal Ni successfully enters the pore of the support KIT-6, and some of the metal Ni mainly disperses on the KIT-6 surface. As the reduction temperature increases, the Ni particle size gradually increases, which is similar to that of XRD study. This phenomenon is mainly due to the high temperature accelerating the accumulation and migration of metal Ni particles, leading them gradually to increase at high temperature. The particle size of the metal Ni is shown in Table 1.

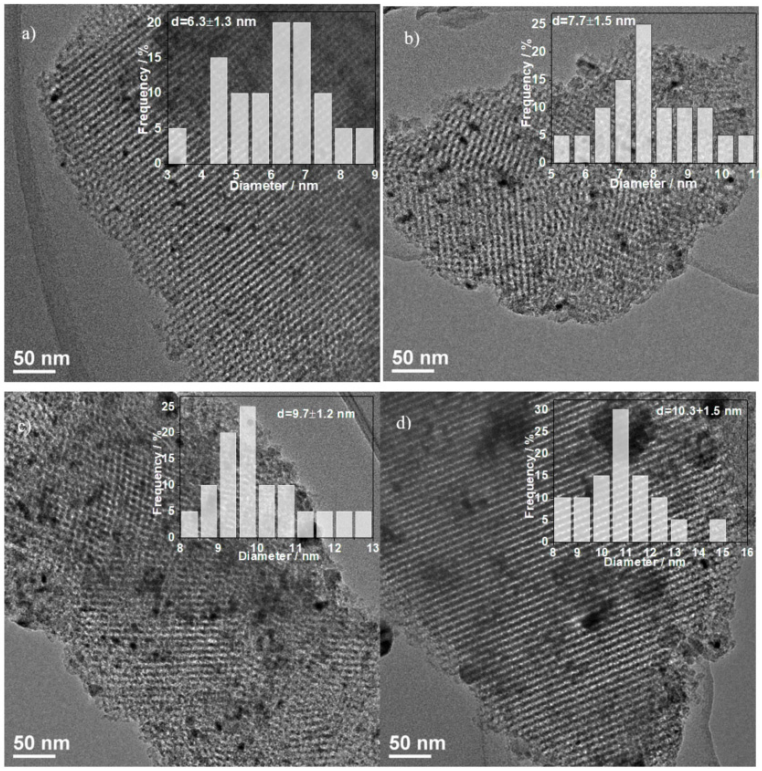

Figure 6. TEM patterns of the studied catalysts: (**a**) 400, (**b**) 450, (**c**) 500, and (**d**) 550.

2.7. Catalytic Activity Test

The prepared RT400, RT450, RT500, and RT550 catalysts exhibit good catalytic HDO performance and ethyl acetate (EA) catalytic HDO activity and product selectivity, as shown in Figure 7a–d. The catalytic HDO performances of the studied catalysts are obviously influenced by the reduction temperature, which are mainly reflected in the complete conversion temperature (T_{100}) of reactant and selectivity of the product (S). The reduction temperature has a significant effect on the catalytic performance. The T_{100} is 300 °C on the RT450 catalyst; the T_{100} of RT400 and RT500 catalysts rise to 320 °C, while the T_{100} of RT550 catalyst further increases to 340 °C. When the reaction temperature is 220 °C, the RT450 catalyst has the highest S_{ethane}, which is 86.9%; among the RTx catalysts at this point, a small amount of ethanol is detected, $S_{ethanol}$ is 6.7%. However, the intermediate product ethanol can be completely transformed at 240 °C. S_{ethane} can reach 96.8%, but $S_{methane}$ is only 3.2% at 300 °C over the RT450 catalyst which shows the best catalytic performance. For RT400 catalyst, at the initial reaction temperature, $S_{ethanol}$ reaches 37%, and the complete conversion temperature of the ethanol is higher by 40 °C than that of the RT450 catalyst. Finally, S_{ethane} is 97.3%, while $S_{methane}$ is just only 2.7% at 320 °C. For RT500 catalyst, $S_{ethanol}$ is more than 13% at the initial temperature of 220 °C, and the complete conversion temperature of the ethanol is the same as that of the RT400 catalyst. At 320 °C, S_{ethane} and $S_{methane}$ are 97.1% and 2.9%, respectively. However, the activity of RT550 catalyst is the poorest. When ethyl acetate completely transforms, the reaction system also has a little ethanol and methane, which are up to 1.5% and 1.3%, respectively. At the beginning of the reaction, in the RT550 catalyst, $S_{ethanol}$ is 30.5 percent points higher than that of RT450 catalyst; conversely, S_{ethane} is 24.1 percent points lower than that of RT450 catalyst at 220 °C.

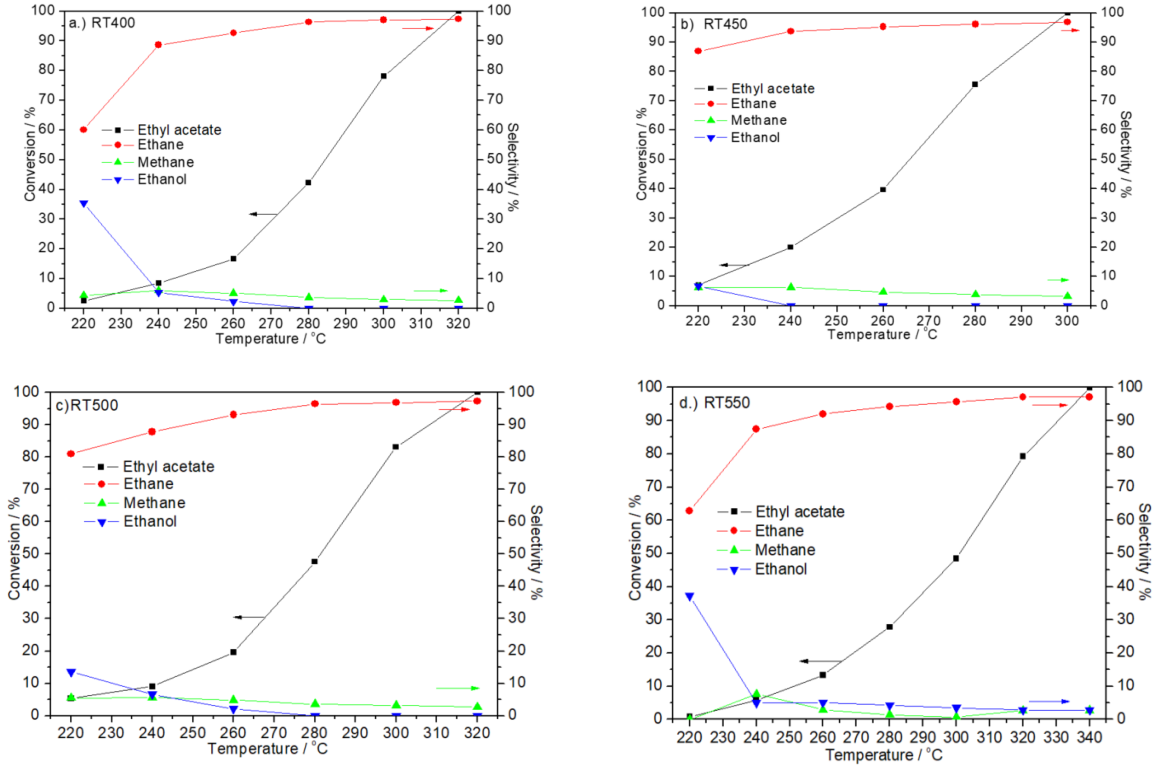

Figure 7. Influence of reduction temperature on the ethyl acetate hydrodeoxygenation conversion and products selectivity over the RTx catalysts. (**a**) RT400, (**b**) RT450, (**c**) RT500, and (**d**) RT550.

In chemical reaction system, the molecules of the reactant can be effectively activated to promote the chemical reaction [33]. Following the general catalytic reaction law, increasing the reaction temperature helps to elevate the energy of the reaction system to accelerate the chemical reaction [34]. Therefore, H_2 molecules are difficult to effectively activate at low reaction temperature, which is not conducive to the formation of reactive H species. When the reaction system energy is low, the activation ability of the corresponding catalyst for the reactants and intermediates is limited. At this time, the intermediate product ethanol hardly achieves further HDO, so the reaction maintains high $S_{ethanol}$ at relative low reaction temperature. The energy of the reaction system increases by enhancing reaction temperature, which accelerates the shift rate of the reactant molecules and the effective collision frequency between activated reactant molecules. Therefore, the HDO reaction of ethyl acetate and intermediate product ethanol can be promoted, and the conversion of ethyl acetate and S_{ethane} can also be significantly improved. Under the studied conditions, ethyl acetate may hydrolyze to produce two intermediate products: acetic acid and ethanol, which can be further deoxygenated to produce ethane [34]. Acetic acid can also react with metallic Ni to produce nickel acetate, and nickel acetate can be further hydrogenated to produce ethane and methane, as shown in Figure S1. At the same time, the ethane molecules can be cracked to methane at a high reaction temperature [25]. In the ester HDO reaction, decarboxylation or decarboxylation can also happen to generate CO_2/CO. The generated CO_2/CO can react with H_2 over the metallic Ni catalyst to produce methane, which is also called methanation reaction [35]. Therefore, the corresponding catalysts show high $S_{methane}$ at studied reaction temperatures.

Based on the results of XRD, NiO species in RT400 catalyst cannot be completely reduced to form metallic Ni species; the result is similar to that of the quasi in situ XPS studies. The content of active centers in the prepared Ni/KIT-6 catalyst is relatively low, which may weaken the ability of the corresponding catalyst to activate H_2 molecules; H_2-TPD can also well confirm the results. In addition, water formed during the HDO reaction could be competing for the active sites together with ethyl acetate as the conversion increases. Moreover, these effects could be enhanced if the Ni particles

are not completely reduced during reaction as water can bind strongly on oxidized metal surfaces. Then, the performance of the RT400 catalyst is weakened. RT450 catalyst, which was obtained by H_2 reduction at 450 °C, shows good HDO performances, and its catalytic performance is obviously higher than that of RT400 catalyst. Compared with RT400, this interesting result can be attributed to the effective reduction of NiO in the precursor of RT450 catalyst. At the same time, quasi in situ XPS confirmed the formation of active metallic Ni in the RT450 catalyst. The crystallinity of the metallic Ni active component is relatively low, and the crystal size is relatively small in RT450 catalyst, which is more conducive to the formation of the catalytic active center. Meanwhile, the smaller crystal size of metallic Ni can also promote the exposure of more active planes to a certain extent, which are conducive to the activation of H_2 molecules and also promote the HDO of reactants and intermediates. Therefore, the RT450 catalyst shows wonderful reactant conversion and S_{ethane}. The catalytic activities of RT500 and RT550 catalysts are significantly poorer than that of RT450 catalyst, and the conversions of ethyl acetate and S_{ethane} continue to decline at low temperature (220–260 °C) by increasing the reduction temperature. This can be attributed to the high reduction temperature resulting in a change in the chemical composition of the catalyst. The samples may even generate new inert crystal planes under high temperature, resulting in a decrease in the ratio of the active crystal planes, which weakens the ability of the corresponding catalyst to activate the reactants. The crystallinities and crystal sizes of metallic Ni in RT500 and RT550 catalysts obviously increase, and the crystal sizes of two catalysts reach 9.1 and 10 nm, respectively. The high crystallinity and large crystal size limit the formation and exposure of the active crystal plane. At first, this weakens the adsorption and activation ability of the active crystal to H_2 molecules; in addition, this hinders the formation or fracture of the "Ni-H" bond. What is more, this weakens the activation capacity of the corresponding catalyst for the "C = O" bond and the "C-O" bond. Therefore, the HDO performance is influenced. According to the results of BET and TEM, the prepared catalysts have large specific surface areas and developed mesoporous structures, which effectively promote the migration and diffusion of gaseous reactant molecules in the pore structure. Therefore, the studied catalysts have perfect catalytic HDO performances.

2.8. Activation Energy Studies

Under the condition of atmospheric pressure and 12,000 mL/h·g_{cat} space velocity, the influence of internal and external diffusion is eliminated as is using the fixed bed reactor to study the mechanism of the prepared RTx catalysts for HDO performance by activation energy experiments. According to the Arrhenius equation, $k = k_0 \cdot \exp(-E_a/RT)$; this equation can be obtained: $\ln k = \ln k_0 - E_a/RT$ (where k_0 is the pre-exponential factor, E_a is the activation energy, R is the gas constant, and T is the thermodynamic temperature). Map the -ln$k$ to T^{-1} over RTx catalysts with different reduction temperature, as shown in Figure 8. From Figure 8, the activation energies of ethyl acetate HDO on RT400, RT450, RT500, and RT550 catalysts are 81.0, 67.7, 79.5, and 90.9 kJ/mol, respectively, according to the slope of the obtained straight line, as shown in Table 2.

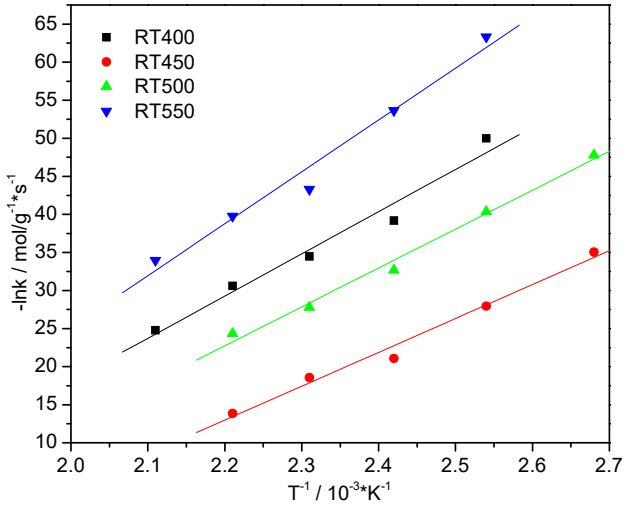

Figure 8. The relationship of ln*k* and T^{-1}.

Table 2. Activation energy studies of RTx catalysts (x = 400, 450, 500, and 550).

Catalysts	Equation	Activation Energy (kJ/mol)
RT400	Y = 9.208X − 12.44	81.0
RT450	Y = 8.066X − 23.17	67.7
RT500	Y = 9.264X − 16.14	79.5
RT550	Y = 11.33X − 9.65	90.9

There are significant differences in the activation energies of the HDO reaction on the studied RTx catalysts, indicating that the changes of the reduction temperatures can further alter the energy barriers over the corresponding catalysts for HDO reaction. In the gas–solid heterogeneous catalytic hydrogenation reaction, the purposes of the adsorption and activation of the reactant molecules on the catalyst surface are to reduce the reaction activation energy. Therefore, the activation energy represents the energy required by the reactant molecules from the normal state to the active state in the chemical reaction under the function of the corresponding catalyst. In other words, under the function of the catalyst, the activation energy, which reflects the difficulty of the catalytic reaction, is the minimum energy needed for the chemical reaction. Meanwhile, chemical reaction rate is closely related to the activation energy. The lower the activation energy is, the faster the reaction rate is; thus, reducing activation energy will effectively promote the reaction rate. Moreover, the reaction system with lower activation energy can ensure that more reactant molecules are activated to form activated molecules, which increases the number of activated molecules, and further, to increase the effective collision probability between the activated molecules, thus accelerating the corresponding chemical reaction rate. According to the XRD and quasi in situ XPS results, the RT400 catalyst obtained by lower temperature reduction has lesser active component, which cannot effectively activate the reactant molecules, thereby elevating the activation energy and the difficulty of corresponding reaction. With the increase of the reduction temperature, even though the content of the active metallic Ni increases, the crystal size of the metallic Ni gradually increases. The large crystal size reduces the number of the exposed active planes on the metallic Ni; then, this action weakens the interaction between catalytic active centers and reactant molecules, which is not conducive to further decreasing the activation energy of ethyl acetate HDO reaction. The increase of crystal size may also lead to the formation of inert crystal plane, which reduces the number of active centers of the corresponding catalyst and affects the activation ability of the studied catalyst to the reactant molecules. Therefore, these adverse factors result in the number of activated molecules in the reaction system being lower and the activation energy of the corresponding reaction being higher. The activation energy of ethyl acetate HDO reaction under the function of RT450 catalyst is lowest among that of the RTx catalysts, and the energy required for

effective collision is lowest. This find shows that the effective activation among the reactant molecules can be realized in the relative lower energy system, thus forming more activated molecules, which is beneficial to the catalytic hydrogenation reaction. At the same time, the lower reaction activation energy leads the formation of active molecules more likely to have effective collisions in the lower energy system, which is beneficial to improve the HDO reaction performance. Hence, decreasing the reaction activation energy can provide an easy way for the ethyl acetate HDO reaction, thus accelerating the reaction to thermodynamic equilibrium. H_2-TPD results also strongly confirm that under the same conditions, RT450 catalyst reaction system has the best adsorption and activation ability for reactant H_2 molecules, thus forming a large amount of reactivated hydrogen species. Effective collisions among activated molecules will help reduce reaction activation energy. This is mainly attributed to the sufficient metallic Ni content, large specific surface area, and suitable crystal size for the RT450 catalyst. The activation energies of the RT500 and RT550 catalysts obtained by enhancing the reduction temperature significantly increase, indicating that the higher the reduction temperature is, the larger the activation energy is. Simultaneously, the BET and TEM results show that the specific surface area of the studied catalyst slightly decreased with the increase of the reduction temperature. High reduction temperature may accelerate the shrinkage or even collapse of mesorpous structure, which weakens the adsorption and activation ability of reactant molecules in the mesorpous structure of corresponding catalyst, as well as further affects the migration and effective collision of activated molecules in mesorpous structure. The effective collision frequency between activated molecules is reduced, which leads to the difficult ethyl acetate HDO reaction increase, as well as to the increase of activation energy. H_2-TPD also confirms that a series of changes in the chemical composition of the studied catalysts have a significant effect on the adsorption and activation ability for the H_2 molecules. The results show that the chemical composition and particle structure of the studied catalyst have a conspicuous influence on the ethyl acetate HDO reaction. In our previous study, it was also found that ethyl acetate HDO reaction is a structural sensitive reaction [30]. To sum up, the amount of active metallic Ni and its crystal size, as well as other chemical compositions may be important reasons for the change of activation energy of RTx series reaction system. The activation energy of the Ni/KIT-6 catalysts prepared at different reduction temperatures for ethyl acetate HDO reaction has the lowest value. The activation energies of the prepared catalysts obey the following order: RT550 > RT400 > RT500 > RT450.

3. Materials and Methods

3.1. Catalyst Preparation

The Ni/KIT-6 catalyst was prepared by impregnation method. KIT-6, which is prepared following the procedure described by our subject group [36,37], was used as the support for the Ni/KIT-6 catalysts. 0.62 g $Ni(NO_3)_2{\cdot}6H_2O$ (Chengdu Kelong Chemical Reagent Factory, China) was dissolved in deionized water with HNO_3. KIT-6 (0.38 g) was added. The sample continued to dry overnight in an oven and then calcined at 550 °C for 4.0 h in air. Finally, the obtained catalyst precursor was subjected to hydrogen reduction 2.0 h to produce the Ni/KIT-6 catalyst at 400, 450, 500, and 550 °C, which were labeled as RT400, RT450, RT500, and RT550, respectively.

3.2. Catalyst Characterization

3.2.1. XRD Characterization

X-ray diffraction (XRD) pattern were record on a Shimadzu-6100 diffractometer (Tokoyo, Japan) with a rotating anode using Ni filtered Cu Ka radiation at 40 kV of a tube voltage and 30 mA of a tube current. The data of 2θ from 20° to 80° range were collected with the step size of 0.02 at the rate of 3°/min, according to our preview work [24].

3.2.2. Quasi In-Situ XPS Studies

The prepared RTx catalyst samples (x = 400, 450, 500, and 550) were in situ reduced in a pretreatment chamber in high purity hydrogen at 400 °C for 60 min to obtain RTx catalysts, and then, obtained RTx catalysts were cooled down to room temperature. Then, the RTx catalysts were directly moved to analysis chamber without being exposed to the environment to analyze the Ni 2p message. The chemical states of the RTx (x = 400, 450, 500, and 550) samples were determined using in situ X-ray photoelectron spectra (in situ XPS). The XPS signals were collected using an ESCALAB 250Xi analyzer (Thermo Fisher Scientific, MA, USA).

3.2.3. BET Characterization

The Brunauer–Emmett–Teller (BET) analysis of the catalysts was determined by N_2 adsorption–desorption using an ASAP 3020 (Micromeritics, GA, USA) instrument. The catalysts were outgassed at 300 °C for 3.0 h before being subjected to N_2 adsorption, according to our preview work [24].

3.2.4. H_2-TPD/R Studies

Temperature-programmed desorption of H_2 (H_2-TPD) was tested on a self-made instrument, the steps follows: 50 mg of catalyst precursor was placed in a quartz U-tube reactor. The catalyst precursors were reduced with a 5% H_2/Ar mixture (25 mL/min) at 400, 450, 500, and 550 °C for 2.0 h, respectively. Afterward, the catalyst is flushed with Ar flow (25 mL/min) to remove all physically adsorbed molecules. The studied catalysts were then heated at 10 °C/min to 700 °C with pure Ar at a flow rate of 25 mL/min. The hydrogen desorption signals were monitored using a thermal conductivity detector (TCD), according to our previous work [24].

3.2.5. TEM Characterization

The transmission electron microscopy (TEM) was performed using a FEI Tecnai G^2 F30 microscope (Oregon, OR, USA) operating at an acceleration voltage of 300 KV.

3.2.6. Catalytic Activity Measurement

Catalytic tests of all the studied catalysts were carried out in a tubular, continuous-flow, fixed-bed reactor under atmospheric pressure. The quartz tube reactor containing 50 mg of the supported nickel oxide precursors were placed inside the tubular furnace. High-purity hydrogen was flowed downward through the reactor containing the catalyst bed, while an electronic mass flow controller was used to control the hydrogen gas flow rate. The precursors were reduced at 400, 450, 500, and 550 °C at hydrogen flow for 2.0 h, followed by cooling under a H_2 flow to the studied temperature. Catalytic activity tests were performed at temperature range of 220 to 340 °C. The actual reduction and reaction temperatures were measured using a thermocouple which was directly inserted into the catalyst bed and were monitored by a temperature programmable controller at a heating rate of 10 °C/min. The fed gas was obtained by bubbling hydrogen through a saturator, which contains the studied model bio-oil compound ethyl acetate in liquid phase kept at constant temperature to achieve the fed gas mixture consisting of gaseous acetate ester (3.3%) and H_2 (96.7%). The fed gas was led over the catalyst at a flow rate of 10 mL·min^{-1}, which is equivalent to a gas mass space velocity of 12,000 mL/g·h. The gas products were monitored using an on-line gas chromatograph (SC-3000B, Chuanyi Automation CO. LTD, Chongiqng, China), equipped with a FID, according to our preview work [24].

The conversion of reactant and the selectivity of products were calculated according to our previous study [24].

4. Conclusions

A series of Ni/KIT-6 catalysts with a metallic Ni loading of 25 wt.% were prepared at different reduction temperatures. They show good catalytic HDO performance to the model compound ethyl acetate. Ethyl acetate is completely converted, while high S_{ethane}, all greater than 95%, can be maintained. The catalytic performance of RT450 catalyst is the best among the prepared Ni/KIT-6 catalysts. The complete conversion of ethyl acetate can be achieved at 300 °C, S_{ethane} is up to 96.8%, $S_{methane}$ is only 3.2%, and the intermediate product ethanol is completely converted at 240 °C. This is mainly attributed to the abundant metallic Ni content in the RT450 catalyst, the small crystal size, only 7.4 nm. KIT-6 support promotes the highly dispersed Ni components and also promotes the migration and activation of reactant molecules in the pore structure, and the Strong Metal Support Interaction Effect (SMSI). In the range of studied reduction temperature, the mesoporous structure does not change significantly, but the reduction temperature affects the HDO performances of the corresponding catalyst. The adsorption and desorption properties of the prepared catalysts for H_2 molecules are in the following order: RT450 > RT500 > RT550 > RT400, and the order of HDOactivities of the prepared catalysts is consistent with that of H_2 desorption. By calculation, the activation energy of the prepared catalysts obeys the following order: RT550 > RT400 > RT500 > RT450.

Author Contributions: X.Z., S.C., and G.Z. conceived and designed the experiments. X.Z. and G.Z. supervised the study. S.C., F.W., and Z.J. carried out materials syntheses. F.W. and J.R. performed all kinetic degradation tests and related measurements and interpretation of results. All authors discussed the results and co-wrote and edited the manuscript. All authors reviewed and approved the manuscript.

Funding: This research is funded by Scientific and Technological Key Program of Chongqing Municipal Education Commission (KJZD-K201800801, KJZD-M201900802); Science and Technology of Chongqing Municipal Education Commission Funded Research Projects (KJQN20190081).

Acknowledgments: Thank you for the support of Engineering Research Center for Waste Oil Recovery Technology and Equipment (Ministry of Education) in the experimental site and equipment.

Conflicts of Interest: The authors declare no conflict of interest.

References

1. Wang, H.; Li, G.L.; Rogers, K.; Lin, H.F.; Zheng, Y. Hydrotreating of waste cooking oil over supported CoMoS catalyst—Catalyst deactivation mechanism study. *Mol. Catal.* **2017**, *443*, 228–240. [CrossRef]
2. Ameen, M.; Azizan, M.T.; Yusup, S.; Ramli, A.; Yasir, M. Catalytic hydrodeoxygenation of triglycerides: An approach to clean diesel fuel production. *Renew. Sustain. Energy Rev.* **2017**, *80*, 1072–1088. [CrossRef]
3. Arun, N.; Sharma, R.V.; Dalai, A.K. Green diesel synthesis by hydrodeoxygenation of bio-based feedstocks: Strategies for catalyst design and development. *Renew. Sustain. Energy Rev.* **2015**, *48*, 240–255. [CrossRef]
4. Ullah, Z.; Bustam, M.A.; Man, Z.; Khan, A.S.; Muhammad, N.; Sarwono, A. Preparation and kinetics study of biodiesel production from waste cooking oil using new functionalized ionic liquids as catalysts. *Renew. Energy* **2017**, *114*, 755–765. [CrossRef]
5. Farid, M.A.A.; Hassan, M.A.; Taufiq-Yap, Y.H.; Shirai, Y.; Hasan, M.Y.; Zakaria, M.R. Waterless purification using oil palm biomass-derived bioadsorbent improved the quality of biodiesel from waste cooking oil. *J. Clean. Prod.* **2017**, *165*, 262–272. [CrossRef]
6. Jung, J.M.; Lee, S.R.; Lee, J.; Lee, T.; Tsang, D.C.W.; Kwon, E.E. Biodiesel synthesis using chicken manure biochar and waste cooking oil. *Bioresour. Technol.* **2017**, *244*, 810–815. [CrossRef]
7. Tan, Y.H.; Abdullah, M.O.; Nolasco-Hipolito, C.; Zauzi, N.S.A. Application of RSM and Taguchi methods for optimizing the transesterification of waste cooking oil catalyzed by solid ostrich and chicken-eggshell derived CaO. *Renew. Energy* **2017**, *114*, 437–447. [CrossRef]
8. Ling, T.R.; Chang, J.S.; Chiou, Y.J.; Chern, J.M.; Chou, T.C. Characterization of high acid value waste cottonseed oil by temperature programmed pyrolysis in a batch reactor. *J. Anal. Appl. Pyrolysis* **2016**, *120*, 222–230. [CrossRef]
9. Wang, X.M.; Qin, X.L.; Li, D.M.; Yang, B.; Wang, Y.H. One-step synthesis of high-yield biodiesel from waste cooking oils by a novel and highly methanol-tolerant immobilized lipase. *Bioresour. Technol.* **2017**, *235*, 18–24. [CrossRef]

10. Horácek, J.; St'ávová, G.; Kelbichová, V.; Kubicka, D. Zeolite-Beta-supported platinum catalysts for hydrogenation/hydrodeoxygenation of pyrolysis oil model compounds. *Catal. Today* **2013**, *204*, 38–45. [CrossRef]
11. Zeng, Y.; Wang, Z.; Lin, W.G.; Song, W.L.; Christensen, J.M.; Jensen, A.D. Hydrodeoxygenation of phenol over Pd catalysts by in-situ generated hydrogen from aqueous reforming of formic acid. *Catal. Commun.* **2016**, *82*, 46–49. [CrossRef]
12. Lu, J.M.; Faheem, B.M.S.; Heyden, A. Theoretical investigation of the decarboxylation and decarbonylation mechanism of propanoic acid over a Ru(0001) model surface. *J. Catal.* **2015**, *324*, 14–24. [CrossRef]
13. Kubičková, I.; Kubička, D. Utilization of triglycerides and related feedstocks for production of clean hydrocarbon fuels and petrochemicals: A review. *Waste Biomass Valorization* **2010**, *1*, 293–308. [CrossRef]
14. Yang, L.Q.; Carreon, M.A. Effect of reaction parameters on the decarboxylation of oleic acid over Pt/ZIF-67membrane/zeolite 5A bead catalysts. *J. Chem. Technol. Biotechnol.* **2016**, *92*, 52–58. [CrossRef]
15. Di, L.; Yao, S.K.; Guang, S.S.; Wu, J.; Dai, W.L.; Guan, N.J.; Li, L.D. Robust ruthenium catalysts for the selective conversion of stearic acid to diesel-range alkanes. *Appl. Catal. B* **2016**, *201*, 137–149. [CrossRef]
16. Chen, J.Z.; Xu, Q.Y. Hydrodeoxygenation of biodiesel-related fatty acid methyl esters to diesel-range alkanes over zeolite-supported ruthenium catalysts. *Catal. Sci. Technol.* **2016**, *6*, 7239–7251. [CrossRef]
17. Kubicka, D.; Bejblov, M.; Vlk, J. Conversion of vegetable oils into hydrocarbons over CoMo/MCM-41 catalysts. *Top. Catal.* **2010**, *53*, 168–178. [CrossRef]
18. Kovács, S.; Kasza, T.; Thernesz, A.; Horváth, I.W.; Hancsók, J. Fuel production by hydrotreating of triglycerides on NiMo/Al_2O_3/F catalyst. *Chem. Eng. J.* **2011**, *176*, 237–243. [CrossRef]
19. Hachemi, I.; Kumar, N.; Mäki-Arvela, P.; Roine, J.; Peurla, M.; Hemming, J.; Salonen, J.; Murzin, D.Y. Sulfur-free Ni catalyst for production of green diesel by hydrodeoxygenation. *J. Catal.* **2017**, *347*, 205–221. [CrossRef]
20. Hachemi, I.; Jeništová, K.; Mäki-Arvela, P.; Kumar, N.; Eränen, K.; Hemming, J.; Murzin, D.Y. Comparative study of sulfur-free nickel and palladium catalysts in hydrodeoxygenation of different fatty acid feedstocks for production of biofuels. *Catal. Sci. Technol.* **2016**, *6*, 1476–1487. [CrossRef]
21. Aziz, M.A.A.; Jalil, A.A.; Triwahyono, S.; Saad, M.W.A. CO_2 methanation over Ni-promoted mesostructured silica nanoparticles: Influence of Ni loading and water vapor on activity and response surface methodology studies. *Chem. Eng. J.* **2015**, *260*, 757–764. [CrossRef]
22. Zhou, G.L.; Wu, T.; Xie, H.M.; Zheng, X.X. Effects of structure on the carbon dioxide methanation performance of Co-based catalysts. *Int. J. Hydrogen Energy* **2013**, *38*, 10012–10018. [CrossRef]
23. Zhou, G.L.; Wu, T.; Zhang, H.B.; Xie, H.M.; Feng, Y.C. Carbon dioxide methanation on ordered mesoporous Co/KIT-6 catalyst. *Chem. Eng. Commun.* **2014**, *201*, 233–240. [CrossRef]
24. Chen, S.; Pan, X.Y.; Miao, C.X.; Xie, H.M.; Zhou, G.L.; Jiao, Z.J.; Zhang, X.M. Study of catalytic hydrodeoxygenation performance for the Ni/KIT-6 catalysts. *J. Saudi Chem. Soc.* **2018**, *22*, 614–627. [CrossRef]
25. Chen, S.; Miao, C.X.; Luo, Y.; Zhou, G.L.; Xiong, K.; Jiao, Z.J.; Zhang, X.M. Study of catalytic hydrodeoxygenation performance of Ni catalysts: Effects of prepared method. *Renew. Energy* **2018**, *115*, 1109–1117. [CrossRef]
26. Ferencz, Z.; Varga, E.; Puskás, R.; Kónya, Z.; Baán, K.; Oszkó, A.; Erdohelyi, A. Reforming of ethanol on Co/Al_2O_3 catalysts reduced at different temperatures. *J. Catal.* **2018**, *358*, 118–130. [CrossRef]
27. Zhou, G.L.; Liu, H.R.; Cui, K.K.; Xie, H.M.; Jiao, Z.J.; Zhang, G.Z.; Xiong, K.; Zheng, X.X. Methanation of carbon dioxide over Ni/CeO_2 catalysts: Effects of support CeO_2 structure. *Int. J. Hydrogen Energy* **2017**, *42*, 16108–16117. [CrossRef]
28. Zhou, G.L.; Xie, H.M.; Gui, B.G.; Zhang, G.Z.; Zheng, X.X. Influence of NiO on the performance of CoO-based catalysts for the selective oxidation of CO in H_2-rich gas. *Catal. Commun.* **2012**, *19*, 42–45. [CrossRef]
29. Zhou, G.L.; Liu, H.R.; Cui, K.K.; Jia, A.P.; Hu, G.S.; Jiao, Z.J.; Liu, Y.Q.; Zhang, X.M. Role of surface Ni and Ce species of Ni/CeO_2 catalyst in CO_2 methanation. *Appl. Surf. Sci.* **2016**, *383*, 248–252. [CrossRef]
30. Arslan, A.; Dogu, T. Effect of calcination/reduction temperature of Ni impregnated CeO_2-ZrO_2 catalysts on hydrogen yield and coke minimization in low temperature reforming of ethanol. *Int. J. Hydrogen Energy* **2013**, *38*, 7268–7279. [CrossRef]
31. Pauly, N.; Yubero, F.; García-García, F.J.; Tougaard, S. Quantitative analysis of Ni2p photoemission in NiO and Ni diluted in a SiO_2 matrix. *Surf. Sci.* **2016**, *644*, 46–52. [CrossRef]

32. Boudjahem, A.G.; Bettahar, M.M. Effect of oxidative pre-treatment on hydrogen spillover for a Ni/SiO_2 catalyst. *J. Mol. Catal. A* **2017**, *426*, 190–197. [CrossRef]
33. Zhou, G.L.; Gui, B.G.; Xie, H.M.; Yang, F.; Chen, Y.; Chen, S.M.; Zheng, X.X. Influence of CeO_2 morphology on the catalytic oxidation of ethanol in air. *J. Indus. Eng. Chem.* **2014**, *20*, 160–165. [CrossRef]
34. Bie, Y.; Lehtonen, J.; Kanervo, J. Hydrodeoxygenation (HDO) of methyl palmitate over bifunctional Rh/ZrO_2 catalyst: Insights into reaction mechanism via kinetic modeling. *Appl. Catal. A* **2016**, *526*, 183–190. [CrossRef]
35. Kellenberger, A.; Jahne, E.; Adler, H.J.; Khandelwal, T.; Dunscha, L. In situ FTIR spectroelectrochemistry of poly [2-(3-thienyl) ethyl acetate] and its hydrolyzed derivatives. *Electrochim. Acta* **2008**, *53*, 7054–7060. [CrossRef]
36. Tan, X.; Lan, H.; Xie, H.M.; Zhou, G.L.; Jiang, Y. Role of surface oxygen species of mesoporous CeCu oxide catalyst in OVOCs catalytic combustion. *J. Environ. Chem. Eng.* **2017**, *5*, 2068–2076. [CrossRef]
37. Zhou, G.L.; Dai, B.C.; Xie, H.M.; Zhang, G.Z.; Xiong, K.; Zheng, X.X. CeCu composite catalyst for CO synthesis by reverse water–gas shift reaction: Effect of Ce/Cu mole ratio. *J. CO_2 Util.* **2017**, *21*, 292–301. [CrossRef]